


[View Journal Online](#)
[View Article Online](#)

A heterocyclic *N'*-(4-(diethylamino)-2-hydroxybenzylidene)-4-oxopiperidine-1-carbohydrazide Schiff base ligand and its metal complexes: Synthesis, structural characterization, thermal behavior, fluorescence properties, and biological activities

 Gajanan Mahadu Dongare  and Anand Shankarrao Aswar *

Department of Chemistry, Sant Gadge Baba Amravati University, Amravati-444602, Maharashtra State, India

 * Corresponding author at: Department of Chemistry, Sant Gadge Baba Amravati University, Amravati-444602, Maharashtra State, India.
 e-mail: aswaranand@gmail.com (A. Aswar).

RESEARCH ARTICLE



doi 10.5155/eurjchem.13.4.415-425.2337

 Received: 22 August 2022
 Received in revised form: 30 September 2022
 Accepted: 07 October 2022
 Published online: 31 December 2022
 Printed: 31 December 2022

KEYWORDS

 SEM
 X-ray diffraction
 Metal complexes
 Antimicrobial activity
 Fluorescence emission
 Heterocyclic hydrazone

ABSTRACT

A new heterocyclic hydrazone Schiff base ligand, *N'*-(4-(diethylamino)-2-hydroxybenzylidene)-4-oxopiperidine-1-carbohydrazide, (H_2L) was derived by a condensation reaction of 4-oxopiperidine-1-carbohydrazide with 4-(diethylamino)-2-hydroxybenzaldehyde. The ligand reacts with chloride salts of chromium(III), manganese(II), iron(III), cobalt(II), nickel(II), copper(II) and zinc(II) to form metal complexes of $[Cr(L)(Cl)(H_2O)_2]$, $[Mn(HL)(Cl)(H_2O)_2]$, $[Fe(L)(Cl)(H_2O)_2]$, $[Co(HL)(Cl)(H_2O)_2]$, $[Ni(HL)(Cl)(H_2O)_2]$, $[Cu(HL)(Cl)(H_2O)_2]$, $[Zn(L)(H_2O)]$, respectively. The structure of the hydrazone ligand was confirmed by elemental analysis and spectroscopic techniques, viz., FT-IR, 1H NMR, ^{13}C NMR, and LC-MS spectroscopy. The newly synthesized ligand behaves as a tridentate *ONO* donor towards Cr, Mn, Fe, Co, Ni, Cu, and Zn metal ions. The spectral, magnetic moment, and thermal data indicate the octahedral geometry for all metal complexes except for Zn, which has tetrahedral geometry with 1:1 stoichiometry (M:L). ESR study revealed that π -bonding covalency is much stronger than the σ -bonding with axial distortion in the structure. The molar conductivity data suggested the nonelectrolytic nature of the complexes. The powder X-ray diffraction patterns suggest the nanocrystalline nature of the compounds. The SEM micrograph of the ligand significantly differs from its Ni(II) complex indicating coordination of Ni(II) ion to the ligand. The intense fluorescence emitted in the region of $\lambda_{excitation}$ 521 to 524 nm due to the functional fluorophores of the ligand and its manganese (II), chromium(III), cobalt(II), and zinc(II) complexes. Various kinetic parameters such as E_a , ΔS , ΔH , and ΔG of various decomposition steps were calculated from TGA diagrams using Coats-Redfern method and the thermal stability order was found to be $Cr < Fe < Co < Mn = Cu < Zn < Ni$. The antibacterial and antifungal activities of the ligand and its divalent and trivalent metal complexes were performed against the various pathogens viz. *Escherichia coli*, *Salmonella typhi*, *Staphylococcus aureus*, *Bacillus subtilis*, *Candida albicans*, and *Aspergillus niger* with reference to standard antibiotics viz. ofloxacin, azithromycin, and fluconazole. All metal complexes showed promising biological activity as compared with their parent ligand and may be used as a potential antimicrobial candidate in biological science.

 Cite this: *Eur. J. Chem.* 2022, 13(4), 415-425

 Journal website: www.eurjchem.com

1. Introduction

The heterocyclic hydrazone Schiff base ligand plays a significant role in the coordination chemistry, as they easily form more stable complexes with most of the transition metal ions and found extensive applications in the various fields comprising organic synthesis, medicinal chemistry, non-linearity, and superb optical (*i.e.*, absorbance and emission properties) to the supramolecular chemistry [1-4]. The hydrazone Schiff base containing the tridentate moiety of *ONO* active donor sites displayed a versatile class of ligands which have been studied for a long time as potential multifunctional properties due to their structural diversity, tautomerism, reaction conditions, and with good yield. The heterocyclic tridentate hydrazone contains the flexible *ONO* donor atoms in

the carbonyl 'O' and the azomethine 'N', and phenolic 'O' active donor sites. Aroyl hydrazones are having to possess paramount importance due to their molecular modularity, structural flexibility, straightforward synthesis, and thermal stability have been explored as a reason for their diversified potential application [5,6].

The transition metal complexes derived from aroyl hydrazones exhibit very good enzymatic activity and are found very important in organometallic synthesis, analytical chemistry, and medicinal chemistry [6,7]. Furthermore, the tridentate moieties of the Schiff base of hydrazones and their complexes gained more recognition due to their broad-ranging biological properties, antinociceptive, and anti-inflammatory activities [8-10]. Hydrazone compounds containing the azomethine group have shown a significant role in the medicinal

field for the copper and iron chelators *in vivo* [11] and *in vitro* for iron overload treatment [12]. The hydrazone Schiff base ligands derived from salicylaldehyde derivatives are found as well-known as multidentate ligands and possess a broad level of antimicrobial efficiency [13-15].

Recently, the interest has grown up due to the single-step synthetic procedure for hydrazone Schiff base ligands with good yield in the crystalline state and more desirable donating property through the enolate/amide oxygen (nucleophile), azomethine nitrogen (nucleophile), and phenolate oxygen. Additionally, piperidone-based carbohydrazones are known to have strong coordinating properties and complexing ability toward transition-metal ions adopting several geometries, *e.g.*, bidentate, tridentate, or polydentate mode of linkage via *NO*, *ONO*, and *N₂O₄*. Transition metal complexes of Schiff base with carbohydrazone functionalities have of special research interest because of their roles in numerous physico-chemical and broad spectrum of biological properties, and functional fluorescence. Reviewing all above facts and in view of our continuing interest in the hydrazone of ligand, we designed and synthesized *N'*-(4-(diethylamino)-2-hydroxybenzylidene)-4-oxopiperidine-1-carbohydrazone ligand (H₂L) and its complexes of chromium(III), manganese(II), iron(III), cobalt(II), nickel(II), copper(II), and zinc(II) ions. The structure of the ligand and complexes were fully characterized by spectro/analytical techniques and magnetic moments. After complete spectro/analytical characterization, the ligand and its complexes were biologically screened *in vitro* for their antibacterial efficiency using the bacterial cocci of *Escherichia coli* (NCBI-0157), *Salmonella typhi* (NICM-2257), *Staphylococcus aureus* (NDCM-2257), *Bacillus subtilis* (NICM-2477) and fungal species of *Candida albicans* (MTCC-1637) and *Aspergillus niger* (NCIM-1005). In addition to this, thermo-kinetic data, fluorescence emission properties, and surface morphology of complexes have been reported for applications.

2. Experimental

2.1. Reagents and physical measurement methods

Metal chlorides were of AR grade (99%) and purchased from S.D. fine chemicals, India, 4-diethylamino salicylaldehyde (99%) (Alpha Aesar, Great Britain), 1-carboethoxypiperid-4-one (99%) (Avra Synthesis, Hyderabad, India) were used without further purification. The solvents were doubly distilled before use. The elemental analysis (CHN) was carried out on a Carlo-Erba analyzer. The metal content of the complexes was analyzed by the gravimetric method after decomposing the organic moiety by a mixture of HClO₄, H₂SO₄, and HNO₃ (1:1.5: 2.5) and then igniting metal oxide. The molar conductance measurements of a 1×10⁻³ M solution of metal complexes in DMSO at room temperature were carried out using a 180-Elico conductivity bridge. FT-IR spectra of ligand and its metal complexes were recorded on an Alpha-II compact Bruker Advance. IR spectrometer. The magnetic susceptibility of the complexes was measured at ambient temperature with a Sherwood MSB-MK-1 balance. The NMR (¹H, ¹³C) spectra of hydrazone ligand were recorded on a Bruker Advance NMR spectrometer (500 MHz). The HR-Mass spectra of the hydrazone ligand was recorded using a micro-mass spectrophotometer. The absorption spectra have been recorded on a UV-Visible-1800 Shimadzu spectrophotometer in the wavelength range (λ) 250 to 1200 nm. The ESR spectrum of the Cu(II) complex was recorded at 77 K in LNT on a JEOL-ESR spectrophotometer using microwave frequency in the range of 8.750-9.650 GHz. Thermogravimetric analysis (TG/DTG) was carried out in N₂ atmosphere on a TGA-4000 Perkin-Elmer thermal analyzer in the temperature range of 40-800 °C, with a linear heating rate 20 °C/min with precision and accuracy of ±0.8 °C controlled by inbuilt Pyris software for TGA application of

inbuilt electromagnetic compatibility (EMC) facilitated of stable weight calibration. The powder X-ray diffraction patterns of the compounds were recorded on a Miniflex (600) benchtop Rigaku X-ray diffractometer with a scanning range between 10-80°, the scan-axis 2θ/θ. The surface morphology of the hydrazone ligand and its complexes were recorded in 3D mode on JEOL-6390LV SEM(X100-X500) scanning electron microscope at 10 μM at 10 kV. The emission spectra were recorded in the wavelength region of 250-800 nm on a photoluminescence spectrophotometer (PL) Hitachi (F-7000) using a 150 W Xenon lamp. The progress of the reaction for the formation of the ligand was checked by using TLC (Merck's silica plates 60F₂₅₄) and visualized by UV irradiation (254 nm).

2.2. Synthesis

2.2.1. Synthesis of *N'*-(4-(diethylamino)-2-hydroxybenzylidene)-4-oxopiperidine-1-carbohydrazone (H₂L)

The hydrazone Schiff base (H₂L) ligand was synthesized by a reaction of 4-oxopiperidine-1-carbohydrazone (0.315 g, 2.0 mmol) with 4-(diethylamino)-2-hydroxybenzaldehyde (0.3865 g, 2.0 mmol) in 20 mL ethanol with continuous stirring. The catalytic amount of sulfuric acid (1-2 drops) was added to the reaction mixture and refluxed for 3 hours in a water bath. After cooling to room temperature, a bright, spongy yellow product was separated out. The resulting product obtained was filtered, washed with dry ethanol, and finally recrystallized from DMSO, then dried over anhydrous CaCl₂ in a desiccator (Scheme 1).

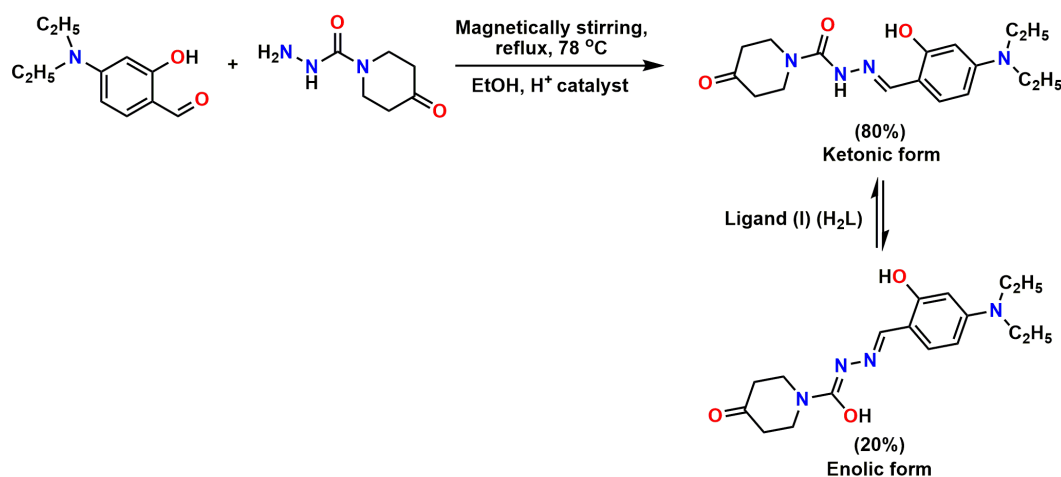
N'-(4-(Diethylamino)-2-hydroxybenzylidene)-4-oxopiperidine-1-carbohydrazone: Color: Yellow. Yield: 80 %. M.p.: 183-185 °C. FT-IR (KBr, ν, cm⁻¹): 3314 (OH, br, phenolic), 3261 (N-H, amide), 1670 (C=O, amide), 1626 (C=N, azomethine), 1300 (C-O, phenolic), 961 (N-N, azomethine). ¹H NMR (500 MHz, DMSO-*d*₆, δ, ppm): 11.48 (s, 1H, Ph-OH), 9.60 (s, 1H, -CH=N-), 8.60 (s, 1H, >NH), 7.41 (d, 1H, Ar-H), 6.55 (d, 1H, Ar-H), 6.11 (s, 1H, Ar-H), 3.49 (dd, 4H, -CH₂-C=O), 3.40 (q, *J* = 3.98 Hz, 4H, >N-CH₂-CH₃), 3.33 (dd, 4H, -CH₂-N), 1.05 (t, *J* = 6.90 Hz, 6H, >N-CH₂-CH₃). ¹³C NMR (125 MHz, DMSO-*d*₆, δ, ppm): 12.30 (1C, CH₃), 12.42 (1C, -CH₃), 39.23 (1C, -CH₂, O=C-CH₂), 39.56 (1C, O=C-CH₂), 43.74 (1C, N-CH₂), 43.99 (1C, N-CH₂), 55.89 (2C, N-CH₂-), 95.79 (1C, Ar-C), 96.92 (1C, Ar-C), 103.93 (1C, Ar-C), 104.34 (1C, Ar-C), 106.27 (1C, Ar-C), 132.90 (1C, HC=N-), 160.48 (1C, C=O, >NHC=O), 162.00 (1C, Ar-C-OH), 180.01 (1C, C=O, H₂C(C=O)CH₂). HRMS (EI, *m/z*) calcd. for C₁₇H₂₄N₄O₃, 332.18; Found [M]⁺¹ = 333.34. Anal. calcd. for C₁₇H₂₄N₄O₃: C, 61.43; H, 7.28; N, 16.86. Found: C, 61.72; H, 7.50; N, 16.90%. UV/Vis (DMSO, λ_{max}, nm, ε): 245 (2.31), 331 (1.673), 432 (0.21).

2.2.2. Preparation of metal complexes

All metal complexes were synthesized by a conventional method. The H₂L ligand (0.6648 g, 2 mmol) and the respective metal chlorides (2 mmol) were dissolved separately in 25 mL of warm DMSO and dry ethanol, respectively. Both solutions were filtered and mixed in warm conditions with continuous stirring. The reaction mixture was then refluxed in an oil bath for about 4 hours and the pH of the reaction mixture was adjusted to *ca.* ~7.0 by adding ethanol: ammonia solution (7:3). The reaction mixture was cooled to room temperature. The colored solid products isolated were collected by filtration, washed with dry ethanol and petroleum ether, and finally dried in a desiccator over anhydrous calcium chloride. The analytical data of the compounds together with their proposed formula are given in Table 1.

Table 1. Analytical and physical data of the compounds.

Compounds	Molecular formula	Molecular weight (g/mol)	Elemental analysis (%)					Metal	Molar conductance ($\Omega^{-1}\text{cm}^2\text{mol}^{-1}$)
			Found, (Calc.)	C	H	N	Cl		
H ₂ L	C ₁₇ H ₂₄ N ₄ O ₃	332.40	61.72 (61.43)	7.50 (7.28)	16.90 (16.86)	-	-	0.0	
[Cr(L)(Cl)(H ₂ O) ₂]	CrC ₁₇ H ₂₆ N ₄ O ₅ Cl	453.86	45.00 (44.99)	6.00 (5.77)	12.50 (12.34)	7.90 (7.81)	12.80 (11.46)	18.20	
[Mn(HL)(Cl)(H ₂ O) ₂]	MnC ₁₇ H ₂₇ N ₄ O ₅ Cl	457.81	44.76 (44.60)	6.00 (5.94)	12.40 (12.24)	7.84 (7.74)	12.15 (12.00)	15.16	
[Fe(L)(Cl)(H ₂ O) ₂]	FeC ₁₇ H ₂₆ N ₄ O ₅ Cl	457.71	44.76 (44.61)	5.85 (5.73)	12.45 (12.24)	7.80 (7.75)	12.30 (12.20)	26.15	
[Co(HL)(Cl)(H ₂ O) ₂]	CoC ₁₇ H ₂₇ N ₄ O ₅ Cl	461.80	44.30 (44.21)	6.10 (5.89)	12.40 (12.13)	7.75 (7.68)	12.84 (12.76)	17.80	
[Ni(HL)(Cl)(H ₂ O) ₂]	NiC ₁₇ H ₂₇ N ₄ O ₅ Cl	461.56	44.35 (44.24)	6.00 (5.90)	12.25 (12.14)	7.78 (7.68)	12.80 (12.72)	21.90	
[Cu(HL)(Cl)(H ₂ O) ₂]	CuC ₁₇ H ₂₇ N ₄ O ₅ Cl	466.42	44.90 (43.78)	6.90 (5.84)	12.15 (12.01)	7.75 (7.60)	13.80 (13.62)	8.15	
[Zn(L)(H ₂ O)]	ZnC ₁₇ H ₂₄ N ₄ O ₄	413.78	49.50 (49.35)	5.90 (5.85)	13.70 (13.54)	-	15.95 (15.80)	6.14	

**Scheme 1.** Synthesis of the ligand and its ketonic-enolic forms.

3. Results and discussion

The reaction between 4-oxopiperidine-1-carbohydrazide and 4-(diethylamino)-2-hydroxybenzaldehyde in ethanol produced new hydrazone, *N'*-(4-(diethylamino)-2-hydroxybenzylidene)-4-oxopiperidine-1-carbohydrazide (H₂L) (Scheme 1). The formation of the ligand was further confirmed by spectro/analytical techniques, *viz.*, FT-IR, ¹H NMR, ¹³C NMR, and HR-MS. The reaction of this ligand with metal chlorides formed two types of complex with good yield [Cr(L)(Cl)(H₂O)₂] (1), [Fe(L)(Cl)(H₂O)₂] (2), and [Zn(L)(H₂O)] (3) in which the hydrazone ligand acts as a dibasic tridentate (in its enolic state) coordinated by *ONO* donor atoms, while in [Mn(HL)(Cl)(H₂O)₂] (4), [Co(HL)(Cl)(H₂O)₂] (5), [Ni(HL)(Cl)(H₂O)₂] (6) and [Cu(HL)(Cl)(H₂O)₂] (7) hydrazone ligand acts as a monobasic-tridentate (in its ketonic form) coordinated by *ONO* donor atoms. All synthesized metal (II) and (III) complexes are colored powder, non-hygroscopic, and stable at room temperature. The complexes are insoluble in water and most of the common organic solvents, but sparingly soluble in DMF and DMSO. The analytical data obtained for the synthesized complexes confirmed that the complexes are mononuclear, and the ligand to metal ratio was found to be 1:1 (M:L) in all complexes. The molar conductivity of metal complexes in DMSO solution (1×10^{-3} M) at room temperature shows low values of 6.14-26.15 $\Omega^{-1}\text{cm}^2\text{mol}^{-1}$ indicating non-electrolytic nature and, moreover, indicated the chloride ion present within the coordination sphere.

3.1. Characterization of the ligand

The proton NMR spectrum of ligand shows a dd at δ 3.40 ppm due to (N-CH₂) protons and a singlet at δ 1.05 ppm for the methylenic protons at α - and β -positions of the (CH₃CH₂)₂N< group. The heterocyclic ring shows two doublets at δ 3.33 ppm for four protons of the -CH₂- group at α -position and another two-doublet appeared at δ 3.49 ppm of four protons another of the -CH₂- group at β -position. One phenolic (OH) and another

one azomethine proton (-HC=N-) showed downfield singlet appears at δ 11.48 and 9.60 ppm, respectively. Aryl protons were observed in their typical δ 6.11-7.41 ppm region. The ¹³C NMR spectrum of the hydrazone ligand exhibits four signals at δ 39.23, 39.56, 43.74 and 43.99 ppm due to the four carbons of the heterocyclic ring. The signal observed at δ 180.01 ppm of the saturated carbonyl carbon of the heterocyclic ring located at low intensity whereas another signal at δ 160.48 ppm is due to amide carbonyl carbon. The azomethine carbon (-HC=N-) signal appeared at δ 132.90 ppm. The aryl carbons appear well within the expected region δ 95.79-106.27 ppm. The separate signals that appeared at δ 12.30 and 12.42 ppm are due to methyl carbon. The HR-Mass spectrum of the ligand shows $M^+ = 333.34$ m/z of its molecular ion peak, considered as to its molecular mass. Some stable fragmented molecular ion species are 260.10 m/z (C₁₃H₁₄N₃O₃⁺) at 100% intensity regarded as a base peak whereas other fragmented species 206.12 m/z and 164.10 m/z indicating (C₁₁H₁₆N₃O⁺) and (C₁₀H₁₄NO⁺) molecular ions, respectively.

3.2. Infrared spectra and bonding mode

In order to ascertain the bonding mode of the hydrazone ligand to the metal ion in the complexes, the infrared spectra of the metal complex were compared with that of its parent ligand. The selected IR bands for the ligand and its complexes together with their assignments are listed in Table 2. The IR spectra impart characteristic bands to identify various functional groups such as carbonyl (C=O), imino (=NH), (C=C), (C-C) bonds, crystal/lattice water, halide linkage, tautomerism, enolic, and phenolic group of vibrations in a heterocyclic ring system. The IR spectrum of the ligand shows a medium broad band at 3314 cm⁻¹ due to the stretching frequency of the phenolic (OH) group and this band has been disappeared from the spectra of all complexes, indicating the formation of a coordination bond between the metal ion and the phenolic oxygen atom *via* deprotonation. It was further confirmed by the upward shifting of stretching frequencies (C-O) by the incre-

Table 2. IR spectral data (cm⁻¹) of the hydrazone ligand and its metal complexes.

Compounds	$\nu(\text{OH})$ phen.	$\nu(\text{NH})$ amide	$\nu(\text{C=O})$	$\nu(\text{C=N})$ azomethine	$\nu(\text{C-O})$ in phenyl	$\nu(\text{C-O})$ in enol	$\nu(\text{N-N})$	Coord. $\nu(\text{H}_2\text{O})$	$\nu(\text{M-O})$	$\nu(\text{M-N})$
H ₂ L	3314	3261	1670	1626	1300	-	961	-	-	-
[Cr(L)(Cl)(H ₂ O) ₂]	-	-	1620	1600	1310	1235	970	850	585	488
[Mn(HL)(Cl)(H ₂ O) ₂]	-	3250	1625	1605	1341	-	958	838	553	440
[Fe(L)(Cl)(H ₂ O) ₂]	-	-	1651	1604	1349	1239	980	840	590	452
[Co(HL)(Cl)(H ₂ O) ₂]	-	3255	1622	1600	1348	-	970	835	560	448
[Ni(HL)(Cl)(H ₂ O) ₂]	-	3248	1630	1600	1312	-	964	820	570	460
[Cu(HL)(Cl)(H ₂ O) ₂]	-	3235	1665	1598	1305	-	972	835	580	474
[Zn(L)(H ₂ O)]	-	-	-	1600	1317	1240	975	850	558	460

Table 3. Magnetic susceptibility and electronic absorbance data of metal complexes.

Metal complexes	$\mu_{\text{effective}}$ (B.M.)	Maximum absorption ν (cm ⁻¹)	Maximum absorption wavelength ν (nm)	Spectral transitions	Ligand fields			Nephelauxetic ratio ($\beta = B/B_0$)
					Dq, (cm ⁻¹)	Interelectronic repulsion B (cm ⁻¹)	Racah parameter B ₀ (cm ⁻¹)	
[Cr(L)(Cl)(H ₂ O) ₂]	3.84	16529 19321 26667	605 518 375	⁴ A _{2g} → ⁴ T _{2g} ⁴ A _{2g} → ⁴ T _{1g} (F) ⁴ A _{2g} → ⁴ T _{1g} (P)	1653	976	918	0.74
[Mn(HL)(Cl)(H ₂ O) ₂]	5.86	10417 11494 20408	960 870 490	⁶ A _{1g} → ⁴ E _g (⁴ D) ⁶ A _{1g} → ⁴ E _g (G) ⁶ A _{1g} → ⁴ T ₂ (G)	1042	667	860	0.77
[Fe(L)(Cl)(H ₂ O) ₂]	5.90	10101 13297 18868	990 752 530	⁶ A _{1g} → ⁴ T _{2g} (G) ⁶ A _{1g} → ⁴ T _{2g} (G) ⁶ A _{1g} → ⁴ E _g (D)	-	-	-	-
[Co(HL)(Cl)(H ₂ O) ₂]	4.62	9346 10787 17575	1070 927 569	⁴ T _{1g} → ⁴ T _{2g} ⁴ T _{1g} → ⁴ A _{2g} ⁴ T _{1g} → ⁴ A _{2g} (F)	1168	704	971	0.73
[Ni(HL)(Cl)(H ₂ O) ₂]	2.80	10256 11163 22173	975 880 451	³ A _{2g} → ³ T _{2g} (F) ³ A _{2g} → ³ T _{1g} (F) ³ A _{2g} → ³ T _{1g} (P)	1026	794	1030	0.77
[Cu(HL)(Cl)(H ₂ O) ₂]	1.71	11073 15384 20408	895 652 490	² B _{1g} → ² A _{1g} (v ₁) ² B _{1g} → ² B _{2g} (v ₂) (CT)	-	-	-	-
[Zn(L)(H ₂ O)]	Dia.	27473 39216	364 255	ILCT (n→π*) ILCT (π→π*)	-	-	-	-

ments of 5 to 49 cm⁻¹ from 1300-1349 cm⁻¹ in all complexes. The phenolic 'O' atom has been involved in the bond formation with metal(II) and metal(III) ions of the complexes. The ligand spectrum displayed a strong characteristic vibrational band at 1626 cm⁻¹, due to $\nu(-\text{HC}=\text{N}-, \text{azomethine})$ and shifting of this band towards lowering frequency by 21-28 cm⁻¹ from 1605-1598 cm⁻¹ in the spectra of Mn(II), Co(II), Ni(II), and Cu(II) complexes indicates the coordination metal atom through azomethine nitrogen. This has been further strengthened by upward the shifting of $\nu(\text{N-N})$ band from 958 to 972 cm⁻¹ in the spectra of the metal complexes. The ligand shows band at 3261 cm⁻¹ due to the stretching vibration of $\nu(\text{N-H})$ group which appeared almost about at the same position as in the case of Mn(II), Co(II), Ni(II), and Cu(II) complexes indicating non-involvement in the coordination, which confirm the presence of ligand in its ketonic form. This is also further confirmed by the shifting of amide $\nu(\text{C=O})$ to lowering frequency by 5-50 cm⁻¹ from 1625-1665 cm⁻¹ in these complexes, suggesting the coordination of carbonyl oxygen atom to metal ions as such without experiencing the enolization. However, these bands are completely absent in Cr(III), Fe(III), and Zn(II) complexes, which confirmed the *enol* formation act in accordance with the coordination linkages to the metal ion after deprotonation [16,17]. Furthermore, the existence of coordinated water molecules was confirmed by the presence of non-ligand bands 820-850 cm⁻¹, which was further supported by the thermal analysis. The coordination of ligand was further confirmed by the appearance of new weak intensity bands, non-ligand bands in the region of 553-590 and 440-488 cm⁻¹ in the IR spectra of the complexes are assigned to frequencies of $\nu(\text{M-O})$ and $\nu(\text{M-N})$ stretching vibrations, respectively. Based on the above data, all metal complexes were identified as a mononuclear compound displayed on the basis of the characteristics of the vibrational band frequencies [18].

3.3. Room temperature magnetic susceptibility and electronic absorption spectral properties

The structural interpretation for the metal complexes was predicted from their magnetic moment and electronic absorption spectra measured at 300.15 K. The synthesized metal complexes were identified by their characteristic absorption of maxima as well as minima and the data are listed in Table 3.

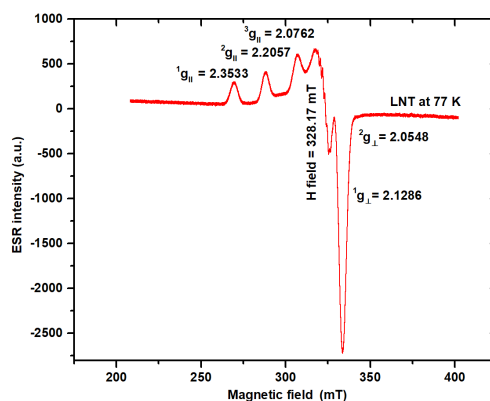
The electronic spectrum of the Cr(III) complex shows three bands at 16529, 19321, and 26667 cm⁻¹ which are assigned to the ⁴A_{2g} → ⁴T_{2g} (v₁), ⁴A_{2g} → ⁴T_{1g} (F) (v₂), and ⁴A_{2g} → ⁴T_{1g} (P) (v₃) transitions, respectively, in accordance with octahedral geometry around chromium ion. The magnetic moment (μ) value is 3.84 B.M., which is indicative of the octahedral geometry. The ligand field parameters such as the crystal field splitting energy (Dq), the Racah parameter (B), the nephelauxetic ratio (β), and the v_2/v_1 were evaluated by using the König equation [19] and values are found to be 1653 cm⁻¹, 676 cm⁻¹, 0.74 and 1.16, respectively, which are also in agreement with the octahedral Cr(III) complexes. The value of interelectronic repulsion parameter B was found to be lower (676 cm⁻¹) than that of the free ion, confirming the presence of covalency in the metal-ligand bond.

The electronic spectrum of the Mn(II) complex exhibits three bands at 10417, 11494, and 20408 cm⁻¹ attributed to ⁶A_{1g} → ⁴E_g (⁴D) (v₁), ⁶A_{1g} → ⁴E_g (G) (v₂), and ⁶A_{1g} → ⁴E_g (G) (v₃) transitions, respectively, in an octahedral geometry. Additionally, the value of magnetic moment 5.86 B.M. is also supported to confirm an octahedral geometry around the Mn(II) ion.

The electronic spectrum of the Fe(III) complex showed three bands located at 10101, 13297, and 18868 cm⁻¹ attributed to the ⁶A_{1g} → ⁴T_{1g} (G) (v₁), ⁶A_{1g} → ⁴T_{2g} (D) (v₂) and ⁶A_{1g} → ⁴E_g (D) (v₃) transitions, respectively, in conformity with octahedral arrangements around the Fe(III) ion and the magnetic moment value is 5.90 B.M. which indicates the presence of the Fe(III) complex in octahedral geometry with d⁵ high spin electronic configuration.

Table 4. Electron spin resonance spectral parameters of Cu(II) complex.

g_e	$g_{ }$	g_{\perp}	g	$\Delta g = g_{ } - g_{\perp}$	G	HSC $\times 10^{-4}$ (cm^{-1})		HSC Avg.	$f = g_{ }/A_{ }$	Bonding parameters		Orbital reduction	
	(Avg.)	(Avg.)	(Avg.)	$A_{ }$		A_{\perp}	α^2			β^2	$K^2_{ }$	K^2_{\perp}	
2.0036	2.211	2.092	2.152	0.119	2.327	148	88	118	149.39	0.77	1.46	0.88	1.55

**Figure 1.** ESR spectrum of Cu(II) complex.

The electronic spectrum of the Co(II) complex exhibits three absorption bands at 9346, 10787, and 17575 cm^{-1} , which have been tentatively assigned to ${}^4T_{1g} \rightarrow {}^4T_{2g}$ (ν_1), ${}^4T_{1g} \rightarrow {}^4A_2$ (ν_2), and ${}^4T_{1g} \rightarrow {}^4T_{1g}$ (F) (ν_3) transitions, respectively, which was in accordance with the octahedral geometry around the cobalt ion. The magnetic moment value 4.62 B.M. indicates octahedral geometry with high-spin arrangements around cobalt ion. The different ligand field parameters such as Dq, B, β , and ν_2/ν_1 have been evaluated and the values are found to be Dq = 1168 cm^{-1} , Racah parameter value (B) = 704 < 971 cm^{-1} (in free ion), β = 0.73 cm^{-1} and ν_2/ν_1 = 1.15. The lower B value of the complex than the free ion value suggests the presence of significant covalency in M-L bonding.

The absorption spectrum of the Ni(II) complex displayed three bands at 10256, 11163, and 22173 cm^{-1} due to ${}^3A_{2g} \rightarrow {}^3T_{2g}$ (F) (ν_1), ${}^3A_{2g} \rightarrow {}^3T_{1g}$ (F) (ν_2) and ${}^3A_{2g} \rightarrow {}^3T_{1g}$ (P) (ν_3) transitions, respectively, characteristic of an octahedral environment for Ni(II) complexes. The observed magnetic moment is 2.80 B.M., which is very close to the spin-only value for two unpaired electrons and is supported for octahedral geometry for the complex. The calculated values of various ligand field parameters were found to be Dq = 1026 cm^{-1} , B = 794 < 1030 cm^{-1} in free ions, and β = 0.77 cm^{-1} are applicable with those of reported for octahedral complexes of Ni(II) [20]. The observed lower value of B than that of the free ion indicates an orbital overlap.

The absorption spectrum of the Cu(II) complex shows a broad absorption band at ~ 11073 cm^{-1} due to the ${}^2B_{1g} \rightarrow {}^2A_{1g}$ transition for distorted octahedral stereochemistry of Cu(II) complexes. The other weak absorption bands observed at 14663, and 20408 cm^{-1} correspond to ${}^2B_{1g} \rightarrow {}^2E_g$ and (L \rightarrow M ion) charge transfer, transitions, respectively. The broadness of band occurs due to the presence of Jahn-Teller distortion, indicating distortion from octahedral geometry. The complex showed a magnetic moment of 1.71 B.M., which indicates the presence of one unpaired electron with the monomeric nature of the complex.

The electronic spectrum of the Zn(II) complex shows two bands at 27473 and 39216 cm^{-1} , which may reasonably be assigned to a charge transfer transition from the ligand to a metal ion. The ligand chromophores transition of $\pi \rightarrow \pi^*$ and $n \rightarrow \pi^*$ group in the UV region. The complex is found to be diamagnetic, as expected for the d^{10} system, which may suggest the tetrahedral geometry around the Zn(II) ion [21].

3.4. ESR study of $[Cu(HL)(Cl)(H_2O)_2]$ complex

The ESR spectrum of the Cu(II) complex exhibits three prominent locations of ($g_{||}$) peaks at 2794, 2981, and 3161 G and another two g_{\perp} peaks at 3336, and 3430 G and the spectrum is shown in Figure 1 and its data are summarized in Table 4. A well-resolved spectrum carrying the electron magnetic tensor components $g_{||} = 2.211$ and $g_{\perp} = 2.092$, which informs the presence of axial symmetry in the complex. The tensor values are shows a ($g_{||} > g_{\perp}$) and the further trend to appears in the order of ($g_{||} > g_{\perp}$) more than free electron magnetic tensor $g_e = 2.0036$ shows the configuration in a $d_{x^2-dy^2}$ orbital in the ground state containing an unpaired electron. It was reported that the $g_{||}$ value is sensitive to the covalency nature of the ligand-metal bond ($g_{||}$ less than 2.3), which indicates that the covalency in the Cu-L bond. The deviation of tensor $g_{ave} = 2.152$ from the free electron tensor value $g_e = 2.0036$ accounted for the covalency in the metal-ligand bond. The geometric parameter was calculated by using Hathway's equation $G = (g_{||} - 2.0023)/(g_{\perp} - 2.0023)$ and found to be 2.327 value which was lower than 4.0 suggesting considerable exchange interaction with the metal center [22]. The tensor (A) displays the most significant tensor properties of magnetic interaction between the electron spin and neighboring nuclear spin, giving rise to the hyperfine structure in the spectrum. The hyperfine splitting constant (HSC) was calculated $A_{||} = 148$ cm^{-1} and $A_{\perp} = 88$ cm^{-1} , which suggesting that electron interaction within the only single copper nucleus confirmed distortion in the octahedral geometry around the Cu(II) ion center. The tensor component 'A' was calculated from the spectra by comparison of the spectral line width and the line shape. The calculated the tensor component ($A_{||} 148$ $\text{cm}^{-1} > A_{\perp} 88$ cm^{-1}) which predicted the distorted octahedral structure with axial symmetry through the copper-O bond and the copper-N bond. Inverse relation of the tensor components $A_{||}$ with $g_{||}$ indicates the conformity of the more delocalization of the electrons in the metal-ligand covalent bond. Comparing the increased values of $A_{||}$ with declining values of $g_{||}$, it clearly indicates more interaction of electrons with its nuclear spin. The ratio (f) = $g_{||}/A_{||}$ was found to be 149.39 and its $A_{avg.} = 118$ which inferred the presence of distortion in the structure. The molecular orbital coefficient was calculated $\beta^2 (1.46) > \alpha^2 (0.77)$ which represents that π -bonding covalency is stronger than the σ -bonding with axial distortion in the structure. The contribution of the orbital reduction parameters ($K^2_{\perp} = 1.55$) > ($K^2_{||} = 0.88$) indicates the greater in-plane π -bonding than the out-of-plane π -bonding [23].



Figure 2. Scanning electron microscopic image of (a) H₂L and (b) Ni(II) complex using JEOL-6390L microscope.

3.5. SEM study

The scanning electron microscopic (SEM) image was captured to compare the surface morphology of the synthesized ligand and its Ni(II) complex as a representative case and is shown in Figures 2a and 2b. The different characteristic shapes and sizes of the ligand particles and its Ni(II) complex provide evidence of the metal complexation. The unit cell of the ligand appears as uniform platelets with slightly varying lateral dimensions to represent the cuboidal shape without any shadows and this was supported by the monoclinic crystal Bravais lattice from XRD studies. The high level of resolution at 500× SEM image of the Ni(II) complex, revealed that morphology appears as a cauliflower-like shape with upper grooves, non-uniform, irregular in shape with aggregation of molecules [24,25]. The magnified pictogram of ligand at ×400 and complex at ×500 level clearly informed differences in shape and size of the particle giving evidence of the formation of the metal complex.

3.6. X-ray diffraction analysis

The powder XRD pattern of H₂L ligand and its derived Mn(II), Ni(II), and Zn(II) metal complexes have been recorded by using the X-ray diffractometer with a target source of copper as an anode material, $\text{CuK}\alpha = 1.540559 \text{ \AA}$. The XRD diffractograms as representative cases to determine the Bravais lattice system, lattice framework, and volume of newly synthesized compounds [26,27]. The prominent peaks of the X-ray diffraction patterns have been indexed to find crystallite size, nature of compounds, peak intensities, relative intensities, interplanar spacing, and unit cell dimensions. Bragg's equation ($n\lambda = 2d\sin\theta$) was used for the evaluation of angle in 2θ and interplanar distances as d . The Miller indices were also reflected in a specified direction, which was supported by the crystal lattice parameters of h , k , and l values. The average particle size was calculated from Scherrer's equation (1918) $L = (K \times \lambda(\text{nm})) / (\beta(2\theta) \times \cos\theta)$; Scherer's constant ($K = 0.9$), peak position in 2θ (deg.), and β parameters of full width at half maximum (FWHM). The ligand and divalent complexes of Mn(II), Ni(II), and Zn(II) were found to be 21.53, 37.030, 39.4341, and 34.89 nm, respectively, which inferring their nanocrystalline nature [28].

3.7. Thermogravimetric analysis

Thermogravimetric analysis is a tool to evaluate the thermal stability of complexes in terms of mass loss with respect to the variation of temperature and provide information about compositions, fragmentation patterns, and the presence of water of hydration as well as crystallization in the complexes. In the present investigation, TG-DTG analysis of the H₂L ligand and its metal complexes was carried out under N₂ atmosphere in the temperature range of 40-800 °C with a linear heating rate 20 °C/min. Thermogravimetric analysis results are summarised in Table 5.

TG plot of ligand shows a one-step decomposition pattern and exhibits a broad endothermic peak (DTG_{max}), i.e., $T_{\text{max}} = 375 \text{ }^\circ\text{C}$, $\Delta H = 196.3 \text{ kJ/mol}$ with mass loss of 63.83% (Theor. 63.87%) due to the loss of one fragmented organic species ($-\text{C}_7\text{H}_{24}\text{N}_4\text{O}_3$). Further continuous heating up to 707 °C, the ligand undergoes complete decomposition and the thermogram becomes horizontal, which may possibly be due to the formation of the carbon residue 33.17% (Theor. 36.13%).

The TG/DTG curve of the $[\text{Cr}(\text{L})(\text{Cl})(\text{H}_2\text{O})_2]$ complex shows a broad peak ($\text{DTG}_{\text{max}} = 130 \text{ }^\circ\text{C}$) in the first decomposition step with a mass loss of 8.40% (Calc. 8.38%) corresponding to the elimination of two coordinated water molecules. In the second stage, a mass loss of 9.09% occurred (Calc. 8.49%) at $\sim 250 \text{ }^\circ\text{C}$ (DTG_{max}) which corresponded to the removal of one mole of chloride ion. In the third stage of degradation, mass loss of the non-coordinated part of the ligand is observed at 62.08% (Calc. 62.04%) at $\sim 450 \text{ }^\circ\text{C}$ and finally, the TG curve attains a horizontal level corresponding to the formation of stable metal oxide ($\frac{1}{2}\text{Cr}_2\text{O}_3$) [29,30].

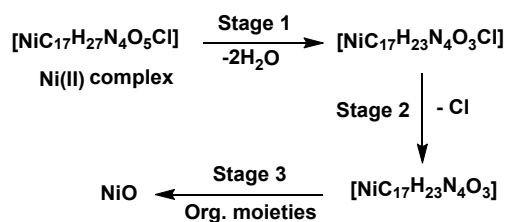
The TG/DTG curve of the $[\text{Mn}(\text{HL})(\text{Cl})(\text{H}_2\text{O})_2]$ complex accounted for a mass loss of 8.00% (Calc. 7.86%) at $\sim 110 \text{ }^\circ\text{C}$ (broad, DTG_{max}), due to the removal of coordinated water ($2\text{H}_2\text{O}$) molecules per mole of complex, whereas in the second decomposition step (DTG_{max}) at 249 °C complex shows a mass loss of 8.68% (Calc. 8.41%) corresponds to the loss of one chloride ion. The third decomposition step was observed around at $\sim 390 \text{ }^\circ\text{C}$ with a mass loss of 75.57% (Calc. 74.00%) corresponding to the left of the maximum part of the coordinated ligand. At the end of the thermogram, it attains a horizontal plateau with residue left about 7.75% (Calc. 9.73%) as a stable metal oxide.

The thermogram of the $[\text{Fe}(\text{L})(\text{Cl})(\text{H}_2\text{O})_2]$ complex exhibits mass loss $\sim 7.86\%$ (calc. 7.86%) at 100 °C broad (DTG_{max}) which is attributed to the loss of two coordinated water molecules from its coordination, while in 2nd step of decomposition at temperature 260 °C (DTG_{max}) with a mass loss 7.94% (Calc. 7.92%) corresponding to the elimination of one-mole chloride molecule. The 3rd stage of pyrolysis was observed at 360 °C with a mass loss of 64.24% (Calc. 64.22%), which was attributed to the elimination of organic parts and was found at 20.01% (Calc. 20.00%) left as a $\frac{1}{2}\text{Fe}_2\text{O}_3$ residue.

The TG/DTG curve of the $[\text{Co}(\text{HL})(\text{Cl})(\text{H}_2\text{O})_2]$ complex shows three steps decomposition in the temperature range of 45-750 °C. The first step of pyrolysis at 130 °C shows a mass loss of 5.98% (Calc. 7.77%) due to the loss of two coordinated molecules from its coordination sphere, whereas, in the second step, DTG_{max} at $\sim 250 \text{ }^\circ\text{C}$ with a loss of mass of 7.82% (calc. 8.33%) corresponds to one molecule of chloride ion. With continued further heating, 3rd stage pyrolysis occurred within the temperature range between 320-600 °C with a maximum mass loss of 62.5% (Calc. 61.76%) corresponding to the organic parts of ligand. At the end of the thermal reaction, the formation of cobalt oxide was 23.70% (Calc. 22.14%).

Table 5. Stepwise thermal analysis data of the ligand and its metal(II/III) complexes.

Compounds	TG range (°C)	Derivative TG (°C)	Mass loss (%)		Fragmented species / Residue assignments
			Experimental	Theoretical	
H ₂ L	44-375	375	66.83	63.87	Removal of C ₇ H ₂₄ N ₄ O ₃ species Organic residues
	375-707	-	33.17	36.13	
[Cr(L)(Cl)(H ₂ O) ₂]	45-130	130	8.40	8.38	Removal 2×H ₂ O molecules
	130-252	249	9.10	9.09	Removal of Cl ion
	252-451	451	62.08	62.04	Removal of organic parts
	410-700	-	20.42	20.40	Residue of 1/2Cr ₂ O ₃
[Mn(HL)(Cl)(H ₂ O) ₂]	45-110	110	8.00	7.86	Removal of coordinated 2×H ₂ O molecules
	110-255	249	8.68	8.41	Removal of one Cl ion
	255-380	379	75.57	74.00	Removal of organic parts
	380-700	-	7.75	9.73	Residue of MnO
[Fe(L)(Cl)(H ₂ O) ₂]	45-110	100	7.86	7.86	Removal of coordinated 2×H ₂ O molecules
	110-390	260	7.94	7.92	Removal of Cl ion
	390-610	390	64.24	64.22	Removal of organic parts
	610-800	-	20.01	20.00	Residue of 1/2Fe ₂ O ₃
[Co(HL)(Cl)(H ₂ O) ₂]	45-110	130	5.98	7.77	Removal of coordinated 2×H ₂ O molecules
	110-252	251	7.82	8.33	Removal of Cl ion
	252-320	320	62.50	61.76	Removal of organic parts
	320-807	-	23.70	22.14	Residue of CoO
[Ni(HL)(Cl)(H ₂ O) ₂]	45-130	100	7.07	7.05	Removal of coordinated 2×H ₂ O molecules
	130-289	270	12.71	9.60	Removal of Cl ion
	289-450	390	64.43	64.25	Removal of organic parts
	450-753	-	15.78	19.10	Residue of NiO
[Cu(HL)(Cl)(H ₂ O) ₂]	45-130	120	7.50	7.49	Removal of coordinated 2×H ₂ O molecules
	130-320	270	8.30	8.22	Removal of Cl ion
	320-630	330	64.20	63.99	Removal of organic parts
	630-776	-	20.00	19.95	Residue of CuO
[Zn(L)(H ₂ O)]	45-240	130	9.97	9.81	Removal of coordinated H ₂ O molecule
	240-650	650	69.01	69.00	Removal of organic parts
	650-750	-	21.02	20.81	Residue of ZnO

**Scheme 2.** Schematic representation of thermal degradation of Ni(II) complex.

The TG/DTG curve of the [Ni(HL)(Cl)(H₂O)₂] complex showed three intense (DTG_{max}) endothermic peaks at 100, 270, and 390 °C exhibiting three-stage decomposition DTG_{max} at 100 °C with a loss of mass of 7.07% (Calc. 7.05%) with the removal of two coordinated molecules, in the 2nd step decomposition, at 270 °C with a mass loss 12.71 % (Calc. 9.60%) by the removal of fragments of one chloride ion. The 3rd degradation stage at 390 °C shows a maximum mass loss of 64.43% (Calc. 64.25%) of the organic parts of the ligand. The residue was left as NiO with 15.78% (Calc. 19.10%). The thermal degradation pattern for the Ni complex is presented in Scheme 2.

The TG curve of [Cu(HL)(Cl)(H₂O)₂] complex shows a mass loss of 7.50% (Calc. 7.49%) at 120 °C, which accounted for the loss of two coordinated water molecules. The second step involves a mass loss of 8.30% (Calc. 8.22%) at DTG_{max} = 270 °C and this may attribute a loss of one chloride ion. In third decomposition step, involves a mass loss of 64.20% (Calc. 63.99%), at 330 °C which confirms the loss of organic parts of ligand, and finally, the thermogram became horizontal which possibly indicates the formation of stable copper oxide residue 20.00% (Calc. 19.95%).

The [Zn(L)(H₂O)] complex displayed two-stage decomposition in which one small and another broad decomposition DTG_{max} at 130 °C for loss of one water coordinated/lattice water 9.97% (Calc. 9.81%) and the loss of organic moiety DTG_{max} at 650 °C was found (69.01% (Calc. 69.00%) in the temperature range of 400-650 °C. The formation of ZnO as the final residue was found to be 21.02%, nearly equal to the theoretical values (20.81%). The presence of water molecules was confirmed by the appearance of IR frequencies in the 820-850 cm⁻¹ in the

coordination, as well as the presence of chloride ions, by the Volhard estimation of these metal complexes [31,32].

We have attempted to predict the thermal stability of metal complexes on the basis of third-step decompositions and found to be Co < Cu < Mn < Fe ≅ Ni < Cr < Zn. All the physicochemical studies suggest the structure of three sets of complexes as proposed in Scheme 3.

3.8. Kinetic parameters of thermal decomposition (Coats-Redfern method)

The thermo-kinetic parameters activation energy (E_a), entropy (ΔS), enthalpy (ΔH), and free energy (ΔG) for the thermal decomposition reactions of the complexes were evaluated from the TG curves by using the Coats-Redfern relation, and values are reported in Table 6. The decomposition rate of compounds was depending upon the temperature and complexity of the structure [33]. The degree of thermal decomposition (α) calculated on TG curve by means of

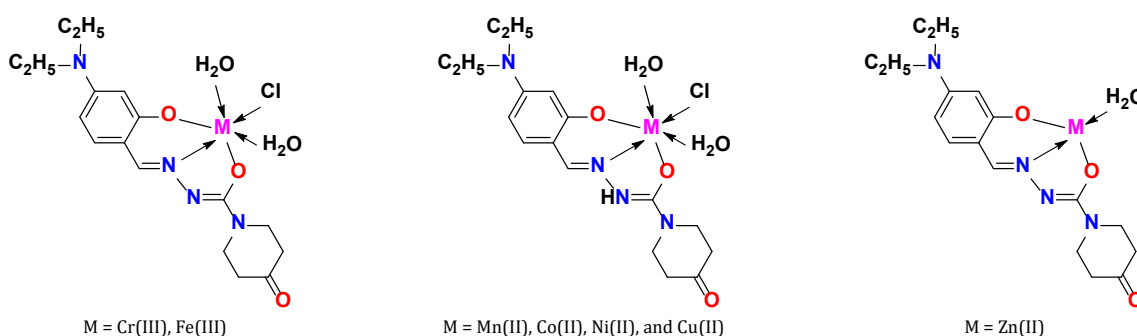
$$\alpha = \frac{W_i - W_t}{W_i - W_f} \quad (1)$$

whereas W_i , W_t , and W_f are the initial weight, final weight, and weight at a time, respectively. The activation energy (E_a) is calculated by Equation (2).

$$\log \frac{[1-\alpha]^{1-n}}{[1-n]} = \frac{E_a}{2.303 \times R \times (T^2 \times S)} \quad (2)$$

Table 6. Calculated thermo-kinetic parameters for thermal degradation data for H₂L ligand and its di- and trivalent metal complexes (Coat-Redfern method).

Compound	Decomposition temperature (°C)	E _a (kJ/mole)	Z (s ⁻¹)	ΔS (J/mol/k)	ΔH (kJ/mole)	ΔG (kJ/mole)
H ₂ L	375	201.64	1.805×10 ²	-16.50	196.3	207.0
[Cr(L)(Cl)(H ₂ O) ₂]	130	10.87	2.01×10 ¹	-11.90	7.50	12.30
	250	23.09	2.11×10 ¹	-13.70	18.70	25.90
	450	140.94	2.34×10 ¹	-15.50	134.90	146.10
[Mn(HL)(Cl)(H ₂ O) ₂]	110	18.80	2.01×10 ¹	-11.50	15.60	20.00
	380	186.32	2.05×10 ¹	-15.70	180.90	191.20
[Fe(L)(Cl)(H ₂ O) ₂]	100	14.22	2.01×10 ¹	-11.30	11.10	15.30
	390	167.29	2.05×10 ¹	-15.90	161.80	172.30
	610	299.00	1.94×10 ¹	-18.70	307.00	290.70
[Co(HL)(Cl)(H ₂ O) ₂]	130	20.81	2.01×10 ¹	-11.90	17.50	22.30
	250	107.69	2.04×10 ¹	-13.90	103.30	110.60
[Ni(HL)(Cl)(H ₂ O) ₂]	100	18.61	2.01×10 ¹	-11.20	15.50	19.70
	270	115.91	2.04×10 ¹	-14.20	111.40	119.10
	390	712.15	2.21×10 ¹	-15.20	706.60	716.70
[Cu(HL)(Cl)(H ₂ O) ₂]	120	12.40	2.01×10 ¹	-11.70	9.10	13.70
	270	91.46	2.03×10 ¹	-14.30	86.90	94.70
[Zn(L)(H ₂ O)]	130	23.09	2.01×10 ¹	-11.90	19.70	24.50
	650	74.11	2.02×10 ¹	-18.80	66.40	83.80

**Scheme 3.** Proposed structure of the metal complexes.

where 'α' denotes the degree of thermal decomposition and its conversion factors for mass losses, 'n' denotes the order of reaction, Gas constant $R = 8.314$ (J/mol) and T^2S (K). The entropy of the thermal reaction was calculated by Equation (3),

$$\text{Entropy } (\Delta S) = 2.303 R \times \log \frac{Z \times h}{K \times T_m} \quad (3)$$

where 'Z' denotes the frequency factor (s⁻¹); h is the Planck's constant (6.63×10^{-34} J.s); k denotes Boltzmann constant (1.3806×10^{-23} J/K); T_m was taken from the peak temperature in K. The enthalpy of reaction (ΔH) is indicating the amount of heat released or absorbed during the reaction and is calculated by Equation (4),

$$\Delta H = E_a - R \times T \quad (4)$$

Another important thermodynamic quantitative property, i.e., free energy change of reaction (ΔG) of a system is calculated with this by Equation (5),

$$\Delta G = \Delta H - T \times \Delta S \quad (5)$$

where ΔH = Heat of reaction, T = Temperature (K), and ΔS = Entropy change. The values of the thermodynamic activation parameters for the ligand and its complexes revealed that the activation energy increased (E_a) 10.87 to 299 kJ/mol, suggesting that the high thermal stability of the compounds may be due to the covalency character of the M-L bond. The negative value of entropy of activation (ΔS) from -11.20 to -18.80 J/mol.K informed that the activated species have more structurally ordered than the dissociated ones and later was slower than the normal reaction rate. The negative values of entropy and the low-frequency factor (Z) were followed in the overall 1st, 2nd and 3rd step and finally resulted in stable metal

oxide formation indicating slow decomposition, non-spontaneous nature and degree of structural 'complexity'. This was also supported by the positive value of the +ve (ΔG) values. The comparative order of parameters follows as $E_a < \Delta G \cong \Delta H$ which correlates with their thermal stability. The values of ΔH and the ΔG of the reaction were found in the range 7.50-706.60, and 13.70-207.00 kJ/mol, respectively, revealing that metal complexes showed more endothermic than exothermic as well as more thermally stable [34].

3.9. Fluorescence spectral study

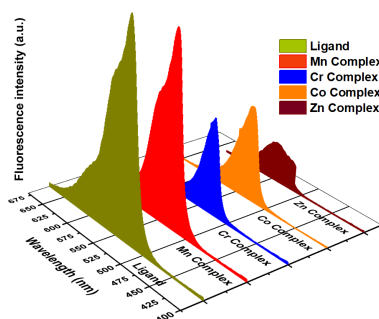
The fluorescence emission spectra of H₂L and its complexes were recorded in the wavelength region of $\lambda = 210$ -810 nm and the emission spectra are presented in Figure 3 and the data in Table 7. At the excitation state, the emitted band was measured in the emission slits having a width of 1.0 nm with the scan speed at a rate of 240 nm/min. The fluorescence emission intensity of the ligand and its [Cr(L)(Cl)(H₂O)₂], [Mn(HL)(Cl)(H₂O)₂], [Co(HL)(Cl)(H₂O)₂] and [Zn(L)(H₂O)₂] complexes were clearly indicated due to the active fluorophores group, i.e. an exchangeable azomethine proton (-CH=N-), functional (C=O) group in heterocyclic rings, the combined inhibition effects of photoinduced electron transfer (PET), static interaction by charge transfer from metal ion to fluorophore groups. The fluorescence emission band of the H₂L ligand and its metal complexes was observed with the varying wavelengths. The compounds have been induced from hyperchromic (blue shift) to bathochromic (red shift) which was resulting the intense fluorescent intensity (I_f) of 120, 109 a.u. at the wavelength $\lambda_{\text{excitation}}$ 527, 524 nm of H₂L ligand and Mn complex, respectively.

Table 7. The fluorescence emission spectral data of the H₂L ligand and its divalent and trivalent metal complexes.

Compounds	Wavelength (nm)	Fluorescence emission intensity (a.u.)
H ₂ L	527	120.0
[Mn(HL)(Cl)(H ₂ O) ₂]	524	109.0
[Cr(L)(Cl)(H ₂ O) ₂]	527	54.43
[Co(HL)(Cl)(H ₂ O) ₂]	530	53.61
[Zn(L)(H ₂ O)]	544	22.74

Table 8. Antibacterial and antifungal assays of the H₂L and its divalent and trivalent metal complexes (mm.)

Compounds	Bacteria (Gram -ve)		Bacteria (Gram +ve)		Fungal species	
	<i>E. coli</i> (NCBI-0157)	<i>S. typhi</i> (NICM-2257)	<i>S. aureus</i> (NDCM-2257)	<i>B. subtilis</i> (NICM-2477)	<i>C. albicans</i> (MTCC-1637)	<i>A. niger</i> (NCIM-1005)
H ₂ L	08	09	10	10	11	09
[Cr(L)(Cl)(H ₂ O) ₂]	10	10	11	12	12	10
[Mn(HL)(Cl)(H ₂ O) ₂]	15	11	09	09	09	10
[Fe(L)(Cl)(H ₂ O) ₂]	11	08	14	10	10	12
[Co(HL)(Cl)(H ₂ O) ₂]	18	15	15	13	20	12
[Ni(HL)(Cl)(H ₂ O) ₂]	16	16	14	19	15	15
[Cu(HL)(Cl)(H ₂ O) ₂]	14	12	12	14	15	18
[Zn(HL)(Cl)(H ₂ O) ₂]	19	20	14	17	25	13
Ofloxacin	30	30	-	-	-	-
Azithromycin	-	-	15	20	-	-
Fluconazole	-	-	-	-	28	30
DMSO	-	-	-	-	-	-

**Figure 3.** Comparative fluorescence emission spectra of the H₂L ligand with its metal(II) and metal(III) complexes.

The other three complexes of Cr, Co, and Zn also emitted significant fluorescent intensity (I_F) as 54.73, 53.61, and 22.74 a.u. at the wavelength of $\lambda_{Excitation}$ 527, 530, and 544 nm, respectively. On the basis of emission intensity of H₂L ligand was shown excellent fluorescent properties than to its divalent and trivalent complexes and displayed the increasing order of Zn < Co < Cr < Mn < H₂L ligand [35,36]. The experimental emission data revealed that the hydrazone compound and its metal(II) and metal(III) complexes are good fluorescent components that may be used in photochemical applications and the detection of heavy metal ions in biological samples. The other Fe, Ni, and Cu complexes of this series were analyzed for fluorescence properties; however, they were referred to as nonfluorescent components due to negligible emission.

3.10. Evaluation of antimicrobial activities

The important aim was to the synthesis of *N'*-(4-(diethyl amino)-2-hydroxybenzylidene)-4-oxopiperidine-1-carbohydra-zide ligand and its metal complexes for testing *in vitro* antibiotic susceptibility for future biological applications. The antimicrobial activities were performed against selected bacterial (cocci) strains (Gram-ve): *Escherichia coli* (NCBI-0157), *Salmonella typhi* (NICM-2257); Gram +ve bacterial cocci: *Staphylococcus aureus* (NDCM-2257), *Bacillus subtilis* (NICM-2477) and fungal species of *Candida albicans* (MTCC-1637), *Aspergillus niger* (NCIM-1005) at a concentration of 1.0 mg/mL employing the disc-diffusion antibiotic culture-base test [37,38]. The culture-based microbiological assay was carried out in the diagnostic laboratory. The DMSO solvent was used as -ve control in the biological reaction. The potentiality of newly synthesized compounds was compared with the standard drugs

viz. ofloxacin, azithromycin, and fluconazole regarded as a +ve control. The inhibition zone growth of microorganisms was studied after ~24 hours of the incubation period. The significant result was found due to the presence of two ethyl groups in the bonding of nitrogen in the amino group, *i.e.* (C₂H₅)₂-N- in all the compounds which lead to decelerating the cluster growth of microorganisms [39]. The antibacterial and antifungal results data of the H₂L hydrazone ligand and its metal(II) and metal(III) complexes are summarized in Table 8. The inhibition zone data suggest pathogenic Gram +ve cocci bacteria, *i.e.* *Staphylococcus aureus* and *Bacillus subtilis* are found more sensitive than Gram -ve cocci bacteria *viz.* *Escherichia coli* and *Salmonella typhi*. Such group specificity may be due to an increase in lipophilicity upon complex formation. The coordination of metal ions increases activity upon coordination with the H₂L ligand was described on account of Tweedy's theory of chelation [40,41]. The partial sharing of the metal(II) and metal(III) ions with the ligand results the in the reduction of polarity which increases lipid solubility and leads to favor in entering into the normal cell of microorganisms [42,43]. Within the fungi, *Candida albicans* are moderately active compared to *Aspergillus niger*. The group of azomethine (C=N) acting in the exchanging of the proton to the metal complexes enhances the destroying capacity of the pathogenic microbial colonies of clusters and chain forms. It was found that the Cu complex played as a competent agent among all compounds inhibiting the growth of *A. niger* from the fungal species. The Co complex showed better activity than the Ni complex, which may be due to the varied morphological structures of the two fungi. In the antibacterial and antifungal studies of the H₂L ligand and its transition complexes showed a broad spectrum activity by the growing resistance to micro-

organisms and may be used as a potent antimicrobial agent in biological sciences [44-46].

4. Conclusions

The metal(II) and metal(III) complexes were synthesized from the reaction of the heterocyclic *ONO* donor *N'*-(4-(diethyl amino)-2-hydroxybenzylidene)-4-oxopiperidine-1-carbohydrazide ligand and with metal chlorides salts. The structural skeleton of the ligand was confirmed by spectroscopic and analytical methods. The newly synthesized mononuclear transition metal complexes are of three types viz. $[M(L)(Cl)(H_2O)_2]$ [$M = Cr$ and Fe], $[M(HL)(Cl)(H_2O)_2]$ ($M = Mn, Co, Ni,$ and Cu) and $[Zn(L)(H_2O)]$. The spectral, analytical, and thermal analysis data have confirmed the suitable geometry of all new complexes. The infrared spectra, absorption-emission spectra, ESR (Cu complex), and magnetic susceptibility data authenticate that the bonding mode of the H_2L ligand through three donor *ONO* atoms with the metal ion the structure and assigned octahedral structure to each of $[Cr(L)(Cl)(H_2O)_2]$, $[Mn(HL)(Cl)(H_2O)_2]$, $[Fe(L)(Cl)(H_2O)_2]$, $[Co(HL)(Cl)(H_2O)_2]$, $[Ni(HL)(Cl)(H_2O)_2]$, $[Cu(HL)(Cl)(H_2O)_2]$, complexes whereas tetrahedral geometry to the $[Zn(L)(H_2O)]$ complex. On the basis of the ESR spectral data, the Cu(II) complex indicated more the π -bonding covalency than σ -bonding in the octahedral region. The powder XRD study has shown the nanocrystalline nature of the complexes. The kinetic data of thermal decomposition were evaluated from the Coats-Redfern relation, indicating that complexes show more ordered structures and are thermally stable at high temperature. The fluorescence emission spectral data of the four compounds demonstrated good fluorescent components and are recommended for use in photochemical applications. The hydrazone ligand and its metal(II) and (III) complexes show better potential activities in antibacterial screening against species of *Staphylococcus aureus*, *Salmonella typhi*, *Bacillus subtilis*, *Escherichia coli*, and fungal species of *Candida albicans* and *Aspergillus niger*. The zone of inhibition data suggests that all divalent and trivalent metal complexes are exhibiting more broad-spectrum activity than the free hydrazone Schiff base ligand, and are represented as potent antimicrobial agents for biological applications.

Acknowledgements

The authors are grateful to the authorities of Sant Gadge Baba Amravati University, Amravati, for providing necessary laboratory facilities, FT-IR, and TGA. We are thankful to the authorities of the sophisticated instrumentation facility, Chandigarh, for the analysis of the elements, the recording of NMR- $(^1H, ^{13}C)$, HR-Mass spectra, and Scanning microscopic analysis of compounds. We are also grateful to the authorities of the Indian Institute of Technology (IIT), Mumbai, India, for the recording of the ESR spectra and the Central Instrumentation Centre (CIC), Shri Shivaji College of Science, Amravati, for the measurement of UV-Visible and X-ray diffraction spectra.

Disclosure statement

Conflict of interest: The authors declare that they have no conflict of interest. Ethical approval: All ethical guidelines have been adhered. Sample availability: Sample of the compounds are available from the author.


CRedit authorship contribution statement

Conceptualization: Anand Shankarrao Aswar; Methodology: Gajanan Mahadu Dongare; Software: Gajanan Mahadu Dongare; Validation: Anand Shankarrao Aswar; Formal Analysis: Gajanan Mahadu Dongare; Investigation: Gajanan Mahadu Dongare; Resources: Gajanan Mahadu Dongare; Data Curation: Anand Shankarrao Aswar; Writing - Original Draft: Gajanan Mahadu Dongare; Writing - Review and Editing: Gajanan Mahadu Dongare; Visualization: Gajanan Mahadu Dongare; Funding acquisition: Gajanan Mahadu Dongare; Supervision: Anand Shankarrao Aswar; Project Administration: Anand Shankarrao Aswar.

ORCID and Email

Gajanan Mahadu Dongare

 infogmdongare@gmail.com

 <https://orcid.org/0000-0002-3986-9796>

Anand Shankarrao Aswar

 aswaranand@gmail.com

 <https://orcid.org/0000-0003-4368-496X>

References

- Backes, G. L.; Neumann, D. M.; Jursic, B. S. Synthesis and antifungal activity of substituted salicylaldehyde hydrazones, hydrazides and sulfohydrazides. *Bioorg. Med. Chem.* **2014**, *22*, 4629–4636.
- John, L.; Joseyphus, R. S.; Joe, I. H. Biomedical application studies of Schiff base metal complexes containing pyridine moiety: molecular docking and a DFT approach. *SN Appl. Sci.* **2020**, *2*, 500.
- Raj, V. A comprehensive review on the pharmacological activity of Schiff base containing derivatives. *Org. Med. Chem. Int. J.* **2017**, *1*, 88–102.
- Hameed, A.; Al-Rashida, M.; Uroos, M.; Abid Ali, S.; Khan, K. M. Schiff bases in medicinal chemistry: a patent review (2010-2015). *Expert Opin. Ther. Pat.* **2017**, *27*, 63–79.
- Barta Holló, B.; Magyari, J.; Armaković, S.; Bogdanović, G. A.; Rodić, M. V.; Armaković, S. J.; Molnár, J.; Spengler, G.; Leovac, V. M.; Mészáros Szécsényi, K. Coordination compounds of a hydrazone derivative with Co(III), Ni(II), and Zn(II): synthesis, characterization, reactivity assessment and biological evaluation. *New J Chem* **2016**, *40*, 5885–5895.
- Govindasami, T.; Pandey, A.; Palanivelu, N.; Pandey, A. Synthesis, characterization and antibacterial activity of biologically important vanillin related hydrazone derivatives. *Int. J. Org. Chem. (Irvine)* **2011**, *01*, 71–77.
- Kaoukabi, H.; Kabri, Y.; Curti, C.; Taourirte, M.; Rodriguez-Ubis, J. C.; Snoeck, R.; Andrei, G.; Vanelle, P.; Lazrek, H. B. Dihydropyrimidinone/1,2,3-triazole hybrid molecules: Synthesis and anti-varicella-zoster virus (VZV) evaluation. *Eur. J. Med. Chem.* **2018**, *155*, 772–781.
- Mistry, S.; Singh, A. K. Synthesis and in vitro antimicrobial activity of new steroidal hydrazone derivatives. *Futur. J. Pharm. Sci.* **2022**, *8*, 7.
- Pape, V. F. S.; Türk, D.; Szabó, P.; Wiese, M.; Enyedy, E. A.; Szakács, G. Synthesis and characterization of the anticancer and metal binding properties of novel pyrimidinylhydrazone derivatives. *J. Inorg. Biochem.* **2015**, *144*, 18–30.
- Krishnamoorthy, P.; Sathyadevi, P.; Butorac, R. R.; Cowley, A. H.; Bhuvanesh, N. S. P.; Dharmaraj, N. Variation in the biomolecular interactions of nickel(II) hydrazone complexes upon tuning the hydrazide fragment. *Dalton Trans.* **2012**, *41*, 6842–6854.
- Hruby, M.; Martínez, I. I. S.; Stephan, H.; Pouckova, P.; Benes, J.; Stepanek, P. Chelators for treatment of iron and copper overload: Shift from low-molecular-weight compounds to polymers. *Polymers (Basel)* **2021**, *13*, 3969.
- Ponka, P.; Richardson, D. R.; Edward, J. T.; Chubb, F. L. Iron chelators of the pyridoxal isonicotinoyl hydrazone class. Relationship of the lipophilicity of the apochelator to its ability to mobilise iron from reticulocytes in vitro. *Can. J. Physiol. Pharmacol.* **1994**, *72*, 659–666.
- Santiago, P. H. O.; Santiago, M. B.; Martins, C. H. G.; Gatto, C. C. Copper(II) and zinc(II) complexes with Hydrazone: Synthesis, crystal structure, Hirshfeld surface and antibacterial activity. *Inorganica Chim. Acta* **2020**, *508*, 119632.
- Shao, B.; Aprahamian, I. Hydrazones as new molecular tools. *Chem* **2020**, *6*, 2162–2173.
- Liu, C.; Chen, M.-X.; Li, M. Synthesis, crystal structures, catalytic application and antibacterial activities of Cu(II) and Zn(II) complexes bearing salicylaldehyde-imine ligands. *Inorganica Chim. Acta* **2020**, *508*, 119639.
- Bansod, A.; Bhaskar, R.; Ladole, C.; Salunkhe, N.; Thakare, K.; Aswar, A. Mononuclear pyrazine-2-carbohydrazone metal complexes: Synthesis, structural assessment, thermal, biological, and electrical conductivity studies. *Eur. J. Chem.* **2022**, *13*, 126–134.
- Mukhtar, H.; Sani, U.; Shettima, U. A. Synthesis, physico-chemical and antimicrobial studies on metal (II) complexes with Schiff base derived from salicylaldehyde and 2,4-dinitrophenylhydrazine. *Int. Res. J. Pure Appl. Chem.* **2019**, 1–8.
- Martínez, S.; Igoa, F.; Carrera, I.; Seoane, G.; Veiga, N.; De Camargo, A. S. S.; Kremer, C.; Torres, J. A Zn(II) luminescent complex with a Schiff base ligand: solution, computational and solid state studies. *J. Coord. Chem.* **2018**, *71*, 874–889.
- Dianu, M. L.; Kriza, A.; Stanica, N.; Musuc, A. M. Transition metal M(II) complexes with isonicotinoylhydrazone-9-anthraldehyde. *J. Serb. Chem. Soc.* **2010**, *75*, 1515–1531.

- [20]. Kharadi, G. J.; Patel, J. R.; Dholakiya, B. Z. Antituberculosis, antifungal and thermal activity of mixed ligand transition metal complexes. *Appl. Organometal. Chem.* **2010**, *24*, 821–827.
- [21]. Kumar, L. V.; Nath, G. R. Synthesis, characterization and biological studies of cobalt(II), nickel(II), copper(II) and zinc(II) complexes of vanillin-4-methyl-4-phenyl-3-thiosemicarbazone. *J. Chem. Sci. (Bangalore)* **2019**, *131*, 76.
- [22]. Ibrahim, K. M.; Gabr, I. M.; Zaky, R. R. Synthesis and magnetic, spectral and thermal eukaryotic DNA studies of some 2-acetylpyridine- [N-(3-hydroxy-2-naphthoyl)] hydrazone complexes. *J. Coord. Chem.* **2009**, *62*, 1100–1111.
- [23]. Kamalakannan, P.; Venkappayya, D. Spectral, Thermal, and Antimicrobial Studies on the Copper(II), Zinc(II), Cadmium(II), and Mercury(II) Chelates of a New Antimetabolite-5-Dimethylamino methyl-2-Thiouracil. *Russ. J. Coord. Chem.* **2002**, *28*, 423–433.
- [24]. Shakir, M.; Hanif, S.; Sherwani, M. A.; Mohammad, O.; Al-Resayes, S. I. Pharmacologically significant complexes of Mn(II), Co(II), Ni(II), Cu(II) and Zn(II) of novel Schiff base ligand, (E)-N-(furan-2-yl methylene) quinolin-8-amine: Synthesis, spectral, XRD, SEM, antimicrobial, antioxidant and in vitro cytotoxic studies. *J. Mol. Struct.* **2015**, *1092*, 143–159.
- [25]. Selwin Joseyphus, R.; Sivasankaran Nair, M. Synthesis, characterization and antimicrobial activity of transition metal complexes with the Schiff base derived from imidazole-2-carboxaldehyde and glycylglycine. *J. Coord. Chem.* **2009**, *62*, 319–327.
- [26]. Purandara, H.; Foro, S.; Thimme Gowda, B. Comparison of the crystal structures and Hirshfeld surface analysis of five N-(4-methyl benzenesulfonyl)glycine hydrazone derivatives. *Acta Crystallogr. C Struct. Chem.* **2018**, *74*, 1553–1560.
- [27]. Ganguly, S.; Karmakar, S.; Pal, C. K.; Chakravorty, A. Regiospecific oximate coordination at the oxygen site: Ligand design and low-spin MnII and FeII/III species. *Inorg. Chem.* **1999**, *38*, 5984–5987.
- [28]. Xie, L.-Y.; Zhang, Y.; Xu, H.; Gong, C.-D.; Du, X.-L.; Li, Y.; Wang, M.; Qin, J. Synthesis, structure and bioactivity of Ni²⁺ and Cu²⁺ acylhydrazone complexes. *Acta Crystallogr. C Struct. Chem.* **2019**, *75*, 927–934.
- [29]. Yernale, N. G.; Udayagiri, M. D.; Mruthyunjayaswam, B. H. M. Synthesis, characterization, mass spectral fragmentation, thermal study and biological evaluation of new Schiff base ligand and its metal(II) complexes derived from 4-(diethylamino)salicylaldehyde and thiazole moiety. *Eur. J. Chem.* **2016**, *7*, 56–65.
- [30]. Dgachi, S.; Rahmouni, F.; Soran, A.; Saoudi, M.; Nemes, G.; Naïli, H. A mononuclear Co(II) complex: Crystal structure, thermal behavior, optical properties and biological activities. *J. Mol. Struct.* **2021**, *1244*, 130996.
- [31]. Al-Hazmi, G. A.; El-Asmy, A. A. Synthesis, spectroscopy and thermal analysis of copper(II) hydrazone complexes. *J. Coord. Chem.* **2009**, *62*, 337–345.
- [32]. Taghizadeh, L.; Montazerzohori, M.; Masoudiasl, A.; Joohari, S.; White, J. M. New tetrahedral zinc halide Schiff base complexes: Synthesis, crystal structure, theoretical, 3D Hirshfeld surface analyses, antimicrobial and thermal studies. *Mater. Sci. Eng. C Mater. Biol. Appl.* **2017**, *77*, 229–244.
- [33]. Abdallah, S. M.; Mohamed, G. G.; Zayed, M. A.; Abou El-Ela, M. S. Spectroscopic study of molecular structures of novel Schiff base derived from o-phthaldehyde and 2-aminophenol and its coordination compounds together with their biological activity. *Spectrochim. Acta A Mol. Biomol. Spectrosc.* **2009**, *73*, 833–840.
- [34]. Singh, B. K.; Jetley, U. K.; Sharma, R. K.; Garg, B. S. Synthesis, characterization and biological activity of complexes of 2-hydroxy-3,5-dimethylacetophenoneoxime (HDMAOX) with copper(II), cobalt(II), nickel(II) and palladium(II). *Spectrochim. Acta A Mol. Biomol. Spectrosc.* **2007**, *68*, 63–73.
- [35]. Aysha, T.; Luňák, S., Jr; Lyčka, A.; Hrdina, R. Synthesis, absorption and fluorescence of hydrazone colorants based on pyrrolinone esters. *Dyes Pigm.* **2011**, *91*, 170–176.
- [36]. Devi, J.; Sharma, S.; Kumar, S.; Jindal, D. K.; Dutta, P. P.; Kumar, D. Transition metal (II) complexes of hydrazones derived from tetralone: synthesis, spectral characterization, in vitro antimicrobial and cytotoxic studies. *Res. chem. intermed.* **2021**, *47*, 2433–2467.
- [37]. Joseph, J.; Rani, G. A. Antioxidant and biochemical activities of mixed ligand complexes. *Appl. Biochem. Biotechnol.* **2014**, *172*, 867–890.
- [38]. Babahan, I.; Emirdağ-Öztürk, S.; Poyrazoğlu-Çoban, E. Spectroscopic and biological studies of new mononuclear metal complexes of a bidentate NN and NO hydrazone-oxime ligand derived from egonol. *Spectrochim. Acta A Mol. Biomol. Spectrosc.* **2015**, *141*, 300–306.
- [39]. Dimitrijević, T.; Novaković, I.; Radanović, D.; Novaković, S. B.; Rodić, M. V.; Anđelković, K.; Šumar-Ristović, M. Synthesis, spectral and structural characterization and biological activity of Cu(II) complexes with 4-(diethylamino)salicylaldehyde and α -diimines. *J. Coord. Chem.* **2020**, *73*, 702–716.
- [40]. Sivasankaran Nair, M.; Arish, D.; Johnson, J. Synthesis, characterization and biological studies on some metal complexes with Schiff base ligand containing pyrazolone moiety. *J. Saudi Chem. Soc.* **2016**, *20*, S591–S598.
- [41]. Panchal, P. K.; Pansuriya, P. B.; Patel, M. N. In-vitro biological evaluation of some ONS and NS donor Schiff's bases and their metal complexes. *J. Enzyme Inhib. Med. Chem.* **2006**, *21*, 453–458.
- [42]. Chang, E. L.; Simmers, C.; Knight, D. A. Cobalt complexes as antiviral and antibacterial agents. *Pharmaceuticals (Basel)* **2010**, *3*, 1711–1728.
- [43]. Yadagiri, B.; Holagunda, U. D.; Bantu, R.; Nagarapu, L.; Guguloth, V.; Polepally, S.; Jain, N. Rational design, synthesis and anti-proliferative evaluation of novel benzosuberone tethered with hydrazide-hydrazones. *Bioorg. Med. Chem. Lett.* **2014**, *24*, 5041–5044.
- [44]. Awantu, A. F.; Fongang, Y. S. F.; Ayimele, G. A.; Nantia, E. A.; Fokou, P. V. T.; Boyom, F. F.; Ngwang, C. K.; Lenta, B. N.; Ngouela, S. A. Novel hydralazine Schiff base derivatives and their antimicrobial, antioxidant and antiplasmodial properties. *Int. J. Org. Chem. (Irvine)* **2020**, *10*, 1–16.
- [45]. Anacona, J. R.; Rincones, M. Tridentate hydrazone metal complexes derived from cephalixin and 2-hydrazinopyridine: synthesis, characterization and antibacterial activity. *Spectrochim. Acta A Mol. Biomol. Spectrosc.* **2015**, *141*, 169–175.
- [46]. El-Sherif, A. A.; Shoukry, M. M.; Abd-Elgawad, M. M. A. Synthesis, characterization, biological activity and equilibrium studies of metal(II) ion complexes with tridentate hydrazone ligand derived from hydralazine. *Spectrochim. Acta A Mol. Biomol. Spectrosc.* **2012**, *98*, 307–321.



Copyright © 2022 by Authors. This work is published and licensed by Atlanta Publishing House LLC, Atlanta, GA, USA. The full terms of this license are available at <http://www.eurjchem.com/index.php/eurjchem/pages/view/terms> and incorporate the Creative Commons Attribution-Non Commercial (CC BY NC) (International, v4.0) License (<http://creativecommons.org/licenses/by-nc/4.0>). By accessing the work, you hereby accept the Terms. This is an open access article distributed under the terms and conditions of the CC BY NC License, which permits unrestricted non-commercial use, distribution, and reproduction in any medium, provided the original work is properly cited without any further permission from Atlanta Publishing House LLC (European Journal of Chemistry). No use, distribution or reproduction is permitted which does not comply with these terms. Permissions for commercial use of this work beyond the scope of the License (<http://www.eurjchem.com/index.php/eurjchem/pages/view/terms>) are administered by Atlanta Publishing House LLC (European Journal of Chemistry).